NASA/CR—1999–208643

Longwave Radiative Flux Calculations in the TOVS Pathfinder Path A Data Set

Amita Mehta, General Sciences Corp., Beltsville, MD 20705

Joel Susskind, Goddard Space Flight Center, Greenbelt, MD 20771

National Aeronautics and
Space Administration

Goddard Space Flight Center
Greenbelt, Maryland 20771

September 1999

Available from:

NASA Center for AeroSpace Information
7121 Standard Drive
Hanover, MD 21076-1320
Price Code: A17

National Technical Information Service
5285 Port Royal Road
Springfield, VA 22161
Price Code: A10

Abstract

A radiative transfer model developed to calculate outgoing longwave radiation (OLR) and downwelling longwave surface flux (DSF) from the Television and Infrared Operational Satellite (TIROS) Operational Vertical Sounder (TOVS) Pathfinder Path A retrieval products is described. The model covers the spectral range of 2 to 2800 cm^{-1} in 14 medium resolution spectral bands. For each band, transmittances are parameterized as a function of temperature, water vapor, and ozone profiles. The form of the band transmittance parameterization is a modified version of the approach we use to model channel transmittances for the High Resolution Infrared Sounder 2 (HIRS2) instrument. We separately derive effective zenith angle for each spectral band such that band-averaged radiance calculated at that angle best approximates directionally integrated radiance for that band. We develop the transmittance parameterization at these band-dependent effective zenith angles to incorporate directional integration of radiances required in the calculations of OLR and DSF. The model calculations of OLR and DSF are accurate and differ by less than 1% from our line-by-line calculations. Also, the model results are within 1% range of other line-by-line calculations provided by the Intercomparison of Radiation Codes in Climate Models (ICRCCM) project for clear-sky and cloudy conditions. The model is currently used to calculate global, multiyear (1985–1998) OLR and DSF from the TOVS Pathfinder Path A Retrievals.

1.0 Introduction

Radiative processes are of fundamental importance to the climate system. Outgoing longwave radiation (OLR) emitted to space and downwelling longwave flux at the earth's surface (DSF) are two of the major components of the overall radiative balance of the earth-atmosphere system. It is well recognized that accurate calculations and measurements of these components are crucial in understanding their roles in climate variability.

Several long-term data sets of outgoing longwave radiation are currently available from satellite measurements. The longest data set of OLR is based on the Scanning Radiometer (SR) and Advanced Very High Resolution Radiometer (AVHRR) measurements taken from National Oceanic and Atmospheric Administration (NOAA) polar orbiting satellites. In this case, SR or AVHRR measurements of 10 to 12 μm channel radiances have been converted to OLR by using regression coefficients pre-determined from radiative transfer calculations (Gruber and Krueger, 1984). The NOAA OLR data cover the period between 1974 and present. A similar regression technique to derive OLR from multi-channel High Resolution Infrared Sounder (HIRS) measurements has also been developed by Ellingson et al. (1994).

An OLR data set has also been produced from the Earth Radiation Budget (ERB) measurements taken aboard Nimbus satellites (Jacobowitz et al. 1984). The ERB OLR data cover the period between 1975 and 1992 (see Kyle et al., 1993). Another OLR data set has been derived from the Earth Radiation Budget Experiment (ERBE) instruments flown on board NOAA-9, NOAA-10, and the Earth Radiation Budget Satellite (ERBS) (Barkstrom, 1989 and references therein). In both the ERB and ERBE data sets broad spectral band radiance measurements from the Wide Field of View (WFOV) non-scanner and narrow Field of View (NFOV) scanner instruments have been used to derive two sets of OLR. The ERBE science team also provides estimates of clear-sky values of outgoing longwave radiation (COLR) based on the scanner measurements (Barkstrom et al. 1989). The ERBE scanner OLR and COLR data are considered to be of very good quality in terms of their spatial and temporal coverage and instrument accuracy. But the global ERBE scanner data are available only for the limited time period from February 1985 to May 1989.

OLR, as mentioned above, has been obtained from top-of-atmosphere satellite measurements. DSF, on the other hand, has no significant correlation with the top-of-atmosphere radiation (Ramanathan, 1986), and so far has not been derived directly from satellite measurements. Also, surface-based measurements of global DSF are not possible. A plausible approach to obtain global, long-term DSF is to calculate the DSF from satellite-derived temperature, moisture and cloud information in radiative transfer. For example, Gupta et al. (1992) have developed a parameterization to calculate DSF based on radiative transfer

model calculations using temperature and moisture profiles retrieved operationally from TOVS, and clouds from the International Cloud Climatology Project (ISCCP). Darnell et al. (1992) have used this parameterization to calculate monthly DSF for a limited period.

The present study is an attempt to produce global, long-term records of OLR and DSF based on satellite measurements. As described by Susskind et al. (1997), global multi-year (1985 to 1998) Pathfinder Path A retrieval products derived from the TOVS radiances are currently available. We developed a radiative transfer model to calculate OLR and DSF as a function of relevant geophysical parameters in producing the longwave radiative fluxes in the Pathfinder Path A data set. Using the model and the Path A retrievals, global, twice-daily per satellite fields of OLR, clear sky OLR (COLR), and DSF are calculated and included as a part of the Pathfinder Path A data set. This approach is similar to that of Wu and Susskind (1990), but a new, computationally efficient radiative transfer model with improved accuracy has been developed. Wu and Susskind used monthly mean soundings to calculate monthly mean OLR based on TOVS retrievals, while the Path A OLR, clear sky OLR, and DSF have been calculated on a sounding by sounding basis. Also, Wu and Susskind used a climatological ozone distribution, whereas we use the TOVS ozone retrievals in the calculations.

The objective of the present report is to describe the radiative transfer model that we have developed for the calculation of OLR and DSF using the Path A retrievals. It is well known that calculations of OLR and DSF require integration of radiances arising from numerous spectral lines, and from all zenith and azimuthal directions. Therefore, radiative transfer models are commonly used to estimate OLR and DSF. Most radiative transfer models are developed to calculate longwave flux for spectral bands rather than for monochromatic, individual spectral lines. This is generally accomplished by modeling the atmospheric transmittances for spectral bands. Examples of these are statistical band models (e.g. Briegleb, 1992 and references therein), the correlation k-distribution method (e.g. Lacis and Oinas, 1991), and pre-computed transmittance table look-up methods (see Chou and Kouvaris, 1991 and references therein). The radiative transfer model we developed is a medium spectral resolution band model. In our model, the parameterization used to compute band averaged transmittances as a function of temperature, moisture, and ozone profiles is a refinement of the approach originally used by Susskind et al. (1983) to model channel transmittances for the HIRS2 instrument of TIROS-N. Also, the parameterization methodology is analogous to that used for modeling the TOVS channel transmittance in the analysis of TOVS data in the Pathfinder Path A data set.

In addition to the frequency integration, calculations of OLR and DSF require directional integration. Directional integration of transmittances or spectral radiances is generally carried out by the diffusivity approximation. According to this approximation, it is

assumed that angle-averaged, band-averaged transmittances can be accurately represented by the band-averaged transmittance of a beam along an effective zenith angle θ=52.96°, where $\sec\theta$=1.66 is the well known diffusivity factor. The diffusivity factor was proposed by Elsasser (1942) and has since been used in radiative transfer calculations for meteorological applications (see Goody and Yung, 1989 for a discussion on this topic). In band models where band transmittances are generally parameterized in terms of optical mass (effective absorber amount), this is accomplished by simply multiplying the band optical path by the factor 1.66 in the radiative transfer calculations (Stephens, 1984). In our model we define and obtain an effective zenith angle for each band used in the flux calculation such that the band radiance in that direction, multiplied by π, is essentially the same as the radiance integrated over all angles. The use of effective zenith angles can be thought of as a band-dependent diffusivity approximation.

In this report, we describe the radiative transfer model, including the methodology used to obtain the effective zenith angles. Accuracy of the model used to calculate OLR and DSF is assessed by a comparison with line by line calculations. Moreover, our model calculations of OLR and DSF are compared with a number of other radiative transfer model calculations provided by the Inter-Comparison of Radiative Codes for Climate Modeling (ICRCCM) program (Ellingson et al., 1991). Comparisons of the TOVS Path A OLR with ERBE and AVHRR OLR, and that of Clear-sky OLR with ERBE clear-sky OLR have been presented by Mehta and Susskind (1999). Comparison of the Path A DSF with available surface measurements is underway and will be reported elsewhere.

The radiative transfer model used to calculate OLR and DSF is outlined in section 2. Comparisons of model calculations for various cases with line by line OLR and DSF calculations and with the ICRCCM results are provided in section 3. A summary is given in section 4.

2.0 Overview of the Calculation of Outgoing Longwave And Downwelling Surface Radiation

OLR is the upward thermally emitted flux, $F^{\uparrow}$, at the top-of-atmosphere and DSF is the downward thermally emitted flux, $F^{\downarrow}$, at the surface. These are related to monochromatic radiances according to:

$$OLR = F^{\uparrow} = \int_{\phi=0}^{2\pi} \int_{\theta=0}^{\pi/2} \int_{\nu=0}^{\infty} R_{\nu}^{\uparrow}(\theta,\phi) \sin\theta \cos\theta \, d\theta \, d\phi \, d\nu \qquad 2.1a$$

and

$$DSF = F^{\downarrow} = \int_{\phi=0}^{2\pi} \int_{\theta=0}^{\pi/2} \int_{\nu=0}^{\infty} R_{\nu}^{\downarrow}(\theta,\phi)\sin\theta\cos\theta\, d\theta\, d\phi\, d\nu \qquad 2.1b$$

where θ and ϕ represent zenith and azimuthal angles respectively, $R_{\nu}^{\uparrow}$ is the thermally emitted monochromatic radiance going to space, and $R_{\nu}^{\downarrow}$ is downwelling radiance at the surface at these angles and at wavenumber ν. For a cloud-free atmosphere, with unit surface emissivity, outgoing radiance $R_{\nu}^{\uparrow CLR}$ can be expressed as:

$$R_{\nu}^{\uparrow CLR}(\theta,\phi) = B_{\nu}(T_s)\,\tau_{\nu}^{\uparrow}(P_s,\theta,\phi) + \int_{P_s}^{P_t} B_{\nu}[T(P)]\frac{d\tau_{\nu}^{\uparrow}(P,\theta,\phi)}{dP}\,dP \qquad 2.2a$$

For a cloudy, overcast atmosphere with spectral cloud emissivity ε_{CV}, $R_{\nu}^{\uparrow CLD}$ can be expressed as:

$$R_{\nu}^{\uparrow CLD}(\varepsilon_{cv},\theta,\phi) = \varepsilon_{cv}\left[B_{\nu}(T_c)\tau_{\nu}^{\uparrow}(P_c,\theta,\phi) + \int_{P_c}^{P_t} B_{\nu}[T(P)]\frac{d\tau_{\nu}^{\uparrow}(P,\theta,\phi)}{dP}\,dP\right] + (1-\varepsilon_{cv})R_{\nu}^{\uparrow CLR}(\theta,\phi) \qquad 2.2b$$

if it is assumed that the clouds have a transmissivity given by $(1-\varepsilon_{CV})$. Similarly, downward radiances for a cloud-free atmosphere at the surface, $R_{\nu}^{\downarrow CLR}$, can be expressed as:

$$R_{\nu}^{\downarrow CLR}(\theta,\phi) = \int_{P_t}^{P_s} B_{\nu}[T(P)]\frac{d\tau_{\nu}^{\downarrow}(P,\theta,\phi)}{dP}\,dP \qquad 2.2c$$

and for overcast atmosphere as:

$$R_{\nu}^{\downarrow CLD}(\varepsilon_{cv},\theta,\phi) = \varepsilon_{cv}\left[B_{\nu}(T_b)\tau_{\nu}^{\downarrow}(P_b,\theta,\phi) + \int_{P_b}^{P_s} B_{\nu}[T(P)]\frac{d\tau_{\nu}^{\downarrow}(P,\theta,\phi)}{dP}\,dP\right] + (1-\varepsilon_{cv})R_{\nu}^{\downarrow CLR}(\theta,\phi)\,. \qquad 2.2d$$

In the above equations, T_s is the surface temperature, T_c the cloud-top temperature, T_b the cloud-base temperature, B_{ν} the Planck function evaluated at wavenumber ν, P_t an effective pressure of the top of atmosphere, P_c and P_b the cloud-top and cloud-base pressure, $\tau_{\nu}^{\uparrow}(P,\theta,\phi)$ is the atmospheric transmittance from pressure P to the top of the atmosphere,

and $\tau_v^{\downarrow}(P,\theta,\phi)$ is the transmittance from pressure P to the surface. (Also, note that everywhere in the text, upward pointing arrows represent outgoing radiance or flux at the top-of-atmosphere, and downward pointing arrows represent downward radiance or flux at the surface).

If for a given scene, the cloudy portion of the scene has fractional coverage α, and the clear portion 1- α, then upward and downward radiances for the scene can be expressed as:

$$R_v^{(\uparrow \text{or} \downarrow)} = (1-\alpha\varepsilon_{cv})R_v^{(\uparrow \text{or} \downarrow)}(\theta,\phi)^{CLR} + \alpha\varepsilon_{cv}\, R_v^{(\uparrow \text{or} \downarrow)}(\theta,\phi)^{CLD} \qquad 2.3$$

where $R_v^{(\uparrow \text{or} \downarrow)}(\theta,\phi)^{CLD}$ are the upwelling and downwelling radiances which would arise from the scene if it were covered by a cloud with emissivity of 1, and the parameter $\alpha\varepsilon_c$ is the radiatively effective cloud fraction. Combining Equations 2.1, 2.2, and 2.3, and ignoring the frequency dependence of ε_{cv}, gives:

$$OLR = (1-\alpha\varepsilon_c)F^{\uparrow\,CLR} + \alpha\varepsilon_c F^{\uparrow\,CLD} \qquad 2.4a$$

$$DSF = (1-\alpha\varepsilon_c)F^{\downarrow\,CLR} + \alpha\varepsilon_c F^{\downarrow\,CLD} \qquad 2.4b$$

where $F^{\uparrow CLR}$ and $F^{\downarrow CLR}$ are the top-of-atmosphere upward flux and downward surface flux from the cloud-free portion of the scene, and $F^{\uparrow CLD}$ and $F^{\downarrow CLD}$ are the analogous fluxes which would emerge from the cloudy portion of the scene if the cloud emissivity were 1.

According to the above set of equations, OLR and DSF calculations require integration of radiances over angles θ, and ϕ, and over wavenumber ν. The radiative transfer model we developed accounts for the angle and frequency integrations in the OLR and DSF calculations using the following approximations :

- The radiances are considered to be homogeneous in the azimuthal direction ϕ. They are dependent only on zenith angle θ.
- Integration over the zenith angle is approximated by evaluating radiances within a spectral band at single band dependent effective zenith angle, and multiplying by π to obtain the flux. The effective zenith angle is found from an ensemble of atmospheric profiles such that the angle integrated flux best approximates what would have been obtained if radiances were integrated over all angles (see section 2.2). The effective band zenith angles are found separately for OLR and DSF calculations.

- The spectral range considered for the calculations extends from 2 to 2750 cm^{-1}. The frequency integration is carried out as a summation of fluxes over 14 spectral intervals or bands, with band centers at frequency ν_i. For each interval, representative effective zenith angles $\theta_i^{\uparrow}$ for OLR, and $\theta_i^{\downarrow}$ for DSF calculations are found based on monochromatic radiance calculations. Upward and downward transmittances for each spectral interval are modeled using averages of monochromatic transmittances evaluated at the appropriate effective zenith angle for that interval using a rapid algorithm band transmittance model. In the rapid algorithm, band transmittances $\tau_i^{\uparrow}$ and $\tau_i^{\downarrow}$ are parameterized as a function of temperature profile, water vapor profile, and ozone profile (see Section 2.3).
- The Planck function for a spectral interval is approximated by its value at the center wavenumber of that band, ν_i, such that $B_i(T) = B_i(\nu_i, T)$.

Using these approximations, clear-sky OLR and DSF are evaluated as :

$$F^{\uparrow\,CLR} = \sum_{i=1}^{N} F_i^{\uparrow\,CLR} = \pi\left[\sum_{i=1}^{N} B_i(T_s)\tau_i^{\uparrow}\left(P_s,\theta_i^{\uparrow}\right) + \int_{P_s}^{P_t} B_i[T(P)]\frac{d\tau_i^{\uparrow}\left(P,\theta_i^{\uparrow}\right)}{dP}dP\right] \qquad 2.5a$$

$$F^{\downarrow\,CLR} = \sum_{i=1}^{N} F_i^{\downarrow\,CLR} = \pi\left[\sum_{i=1}^{N}\int_{P_t}^{P_s} B_i\left(T(P)\right)\frac{d\tau_i^{\downarrow}\left(P,\theta_i^{\downarrow}\right)}{dP}\,dP\right] \qquad 2.5b$$

where $\tau_i\left(P,\theta_i^{\uparrow(\downarrow)}\right)$ are the atmospheric transmittances evaluated at band-averaged effective zenith angles $\theta_i^{\uparrow}$ and $\theta_i^{\downarrow}$. Analogous equations can be written for $F^{\uparrow\,CLD}$ and $F^{\downarrow\,CLD}$. An assumption of unit cloud emissivity in the calculation of $F^{\uparrow(\downarrow)\,CLD}$ is made because the cloud emissivity is included in the fractional cloud cover $\alpha\varepsilon_c$ in equations 2.4a-b.

The effective zenith angles and band transmittances are derived from monochromatic, line by line transmittance calculations. In the following sub-sections, the line by line calculations, method of finding the effective zenith angles, and the parameterization of the band transmittances are briefly described.

2.1 Line by line Calculations

Monochromatic line by line (LBL) absorption coefficients used in this study were carried out for a reference climatological profile of temperature, water vapor, and ozone, representing spring time atmospheric conditions at 40°N. The mixing ratios of CO_2, N_2O, and

CH_4 were assumed to be constant with height in this profile, with values given in McClatchey et al. (1972). For the reference profile, LBL calculations of integrated optical depths in 66 atmospheric layers from 0 to 1000 mb were obtained between 0 to 2750 cm^{-1} at every 0.01 cm^{-1} (Susskind and Searl, 1978). Optical depths for two additional temperature profiles, one colder than the reference temperature profile by 20°C and another warmer by the same amount, were also computed. LBL optical depths for any temperature profile were modeled as a quadratic function of temperature based on values calculated for the reference profile and the two additional profiles. Monochromatic optical depths for any water vapor (ozone) profile were computed by multiplying the reference optical depths values by the ratio of the layer water vapor (ozone) column density in the profile to that in the reference profile. The total transmittance function also includes absorption by the Nitrogen continuum and water vapor continuum, as in Susskind and Searl (1978). Monochromatic optical depths at any zenith angle were obtained from the nadir values by multiplying them by secant of the zenith angle.

In order to generate the effective zenith angles and the coefficients of the band transmittance model, 22 different profiles of varying temperature, water vapor, and ozone were used. Monochromatic transmittances (and radiances) for these profiles at eight zenith angles were calculated as described above. The eight angles chosen for the calculations, have been used in the angular integration of radiances by Gaussian quadrature.

2.2 Effective Zenith Angles

To obtain the effective zenith angles for model bands, the concept of monochromatic effective zenith angle is first defined. As mentioned earlier, azimuthal symmetry of radiances is assumed. For a given atmospheric profile n, if the outgoing and downwelling surface radiances were independent of zenith angle and were equivalent to their values at angles $\theta_e^{\uparrow}(\nu,n)$ and $\theta_e^{\downarrow}(\nu,n)$ respectively then:

$$\frac{F_\nu^{\uparrow}}{\pi} = 2R_\nu{}^{\uparrow}\left(\theta_e^{\uparrow}(\nu,n)\right)\int_{\theta=0}^{\pi/2}\sin\theta\cos\theta\,d\theta = R_\nu{}^{\uparrow}\left(\theta_e^{\uparrow}(\nu,n)\right) \qquad 2.6a$$

and

$$\frac{F_\nu^{\downarrow}}{\pi} = 2R_\nu{}^{\downarrow}\left(\theta_e^{\downarrow}(\nu,n)\right)\int_{\theta=0}^{\pi/2}\sin\theta\cos\theta\,d\theta = R_\nu{}^{\downarrow}\left(\theta_e^{\downarrow}(\nu,n)\right) \qquad 2.6b$$

The single profile effective zenith angles, $\theta_e^{\uparrow}(\nu,n)$ and $\theta_e^{\downarrow}(\nu,n)$ are therefore defined so that the radiances $R_\nu^{\uparrow}$ and $R_\nu^{\downarrow}$ calculated at these angles and the actual angle-integrated radiances $F_\nu^{\uparrow}$ and $F_\nu^{\downarrow}$ satisfy Equations 2.6a-b. Radiances generally vary monotonically with zenith

angle, decreasing (increasing) with increasing angle for upwelling (downwelling) flux if the monochromatic radiance is coming from the troposphere. In the case of upwelling radiance, the reverse is true if the radiance is coming from the stratosphere. Consequently, the effective zenith angle at any wavenumber is well defined for a given profile. As described in section 2.1, line by line monochromatic upwelling and downwelling radiances $R_\nu^\uparrow$ and $R_\nu^\downarrow$ for eight Gaussian quadrature angles and corresponding fluxes, $F_\nu^\uparrow$ and $F_\nu^\downarrow$, have been computed at a 0.01 cm^{-1} spectral spacing for 22 atmospheric profiles. Using these calculations, effective zenith angles, $\theta_e^{\uparrow(\downarrow)}(\nu,n)$, for each wavenumber and profile were found by linear interpolation of $R(\theta)$ in cosine(θ), so that $R_\nu^\uparrow$ equals $F_\nu^\uparrow/\pi$ and $R_\nu^\downarrow$ equals $F_\nu^\downarrow/\pi$ for each case. The values of effective zenith $\theta_i^\uparrow$ and $\theta_i^\downarrow$ for the model spectral band i are computed according to:

$$\theta_i^{\uparrow(\downarrow)} = \frac{\sum_{\nu=\nu_1}^{\nu_2}\sum_{n=1}^{22}\theta_e^{\uparrow(\downarrow)}(\nu,n)\frac{dR_\nu^{\uparrow(\downarrow)}(\nu,n)}{d\theta}}{\sum_{\nu=\nu_1}^{\nu_2}\sum_{n=1}^{22}\frac{dR_\nu^{\uparrow(\downarrow)}(\nu,n)}{d\theta}} \qquad 2.7$$

where $\nu 1$ and $\nu 2$ are the lower and upper limits of wave numbers for band i and $\frac{dR_\nu^{\uparrow(\downarrow)}(\nu,n)}{d\theta}$ is the derivative of profile n radiance with respect to angle at the effective zenith angle at each frequency. Equation 2.7 ensures that the profiles and frequencies for which radiances vary most with zenith angles carry appropriately more weight.

Figure 1a shows monochromatic spectral outgoing flux $F_\nu^\uparrow$, and Figure 1b shows the equivalent monochromatic brightness temperature spectrum, given by $\theta_\nu = B_\nu^{-1}\left(\frac{F_\nu}{\pi}\right)$, averaged over the values obtained from the 22 profiles, in the spectral range of 2 to 2750 cm^{-1}. Analogous spectra for the downwelling surface flux $F_\nu^\downarrow$, and corresponding equivalent monochromatic brightness temperature are shown in Figures 1c and 1d. The upwelling flux spectra given in figures 1a and 1b clearly show absorption bands of water vapor, carbon dioxide and ozone, along with atmospheric windows in regions between 800 and 1000 cm^{-1} and between 1050 cm^{-1} and 1200 cm^{-1}. The downwelling flux spectra in Figure 1c and 1d show features which are out of phase with those of the upwelling flux spectrum. As a result of the strong absorption by CO_2 and water vapor near the earth's surface the emission level is close to the surface over most of the spectrum, except in the atmospheric window regions in which the atmosphere is not opaque and some radiative fluxes coming from colder temperatures reach the surface.

Figure 2 shows monochromatic radiances $R_\nu^{\uparrow}(\theta)$ and $R_\nu^{\downarrow}(\theta)$, averaged over the 22 profiles evaluated at each of five different zenith angles in the same spectral range. These angles are a subset of angles used in the angular integration of radiances by Gaussian quadrature. The outgoing radiances (Figure 2 top panel) generally decrease with increasing zenith angle. This is due to increased attenuation of radiation arising from warmer, lower layers in the atmosphere and increased emission from colder, higher layers as angle increases. However, at the wavenumbers where the main emission going to space arises from the stratosphere, e.g. in the center portion of 15 μm CO_2 band, the radiances increase with increasing zenith angle. The downwelling radiances, on the other hand, are independent of zenith angle over most of the spectrum but increase with increasing zenith angle in the atmospheric window region (bottom panel of Figure 2), because as the optical depth increases at higher zenith angles, more downwelling radiation arising from the lower, warmer tropospheric layers reaches the surface.

To give an indication of the corresponding monochromatic effective zenith angles, we define and plot $\theta_e^{\uparrow(\downarrow)}(\nu)$, such that:

$$\theta_e^{\uparrow(\downarrow)}(\nu) = \frac{\sum_{n=1}^{22} \theta_e^{\uparrow(\downarrow)}(\nu,n) \frac{dR_\nu^{\uparrow(\downarrow)}(\nu,n)}{d\theta}}{\sum_{n=1}^{22} \frac{dR_\nu^{\uparrow(\downarrow)}(\nu,n)}{d\theta}} \qquad 2.8$$

These angles are shown in Figure 3. The solid horizontal line in Figure 3 is at 52.96°, which is the frequency independent angle commonly used in the diffusivity approximation. At the frequencies for which the derivative of the radiance with angle is less than $1.0e^{-5}$ $mW \cdot m^{-2} \cdot ster^{-1} \cdot (cm^{-1})^{-1} \cdot degree^{-1}$, the effective angles are not shown in the figure since radiances are almost the same at all angles in these cases and do not contribute to the band-averaged effective zenith angles. As shown in Figure 3, effective zenith angles for outgoing flux $\theta_e^{\uparrow}(\nu)$, in general, remain between 48° to 58° in the large portion of the range 2 to 2750 cm^{-1}. In the window region between 800 to 1250 cm^{-1}, the angles remain approximately between 55° to 58°, except in the ozone absorption band where they are between 40° to 52°. Effective angles in regions of strong water vapor absorption tend to be about 50°, and values in the 15 μm and 4.3 μm CO_2 bands are somewhat lower. The effective zenith angles for downwelling flux, $\theta_e^{\downarrow}(\nu)$, are lower compared to those for outgoing flux. In the case of downwelling flux, emission is primarily coming from the bottom of the atmosphere where lines

are stronger. In frequency regimes in which radiances vary considerably with zenith angles, e.g. between 800 and 1200 cm^{-1}, values of $\theta_e^{\downarrow}(\nu)$ are found to be between 52° to 56°. In the remaining part of the spectrum, where the variation of downwelling radiances with angle is negligible (see Figure 2), effective angles are between 38° to 45°. The major points of interest are that the effective zenith angle varies considerably with frequency, the values differ from 52.96°, and they are different for upwelling and downwelling flux.

The behavior of effective angles can be understood based on how radiances vary with zenith angles. In equation 2.1, if radiances $R_\nu(\theta)$ were linear in $\sec\theta$, it is easy to show that the θ_e is equal to 60°. This would occur if the monochromatic absorption coefficient was small and the atmospheric transmittance can be approximated as linear in the optical path. If $R_\nu(\theta)$ were linear in θ (not a physical situation), then θ_e would be 45°. To the extent that $R_\nu(\theta)$ varies faster than linear in θ, θ_e would be between 45° and 60°. On the other hand, $\theta_e < 45°$ would occur if $R_\nu(\theta)$ varied slower than linear in θ. This can occur for very large absorption features which saturate at intermediate zenith angles.

The 14 bands chosen for the calculations, and the means and standard deviations of the effective zenith angles for these bands based on the 22 profiles, are given in Table 1a for OLR and in 1b for DSF, along with corresponding values of secant(θ_i). As mentioned earlier, for computational purposes, the frequency-independent value of secant(θ)=1.66 is generally used in most radiative transfer models. We find that the band values of secant(θ_i) for OLR range from 1.57 to 1.76, and the average value is close to 1.66. However, for DSF many values of secant(θ_i) are significantly lower than 1.66.

Using the effective zenith angles for each band shown in Table 1, band-averaged transmittances are computed for these angles as a function of the temperature, moisture, and ozone profile using the rapid band transmittance algorithm model as described in the following section.

2.3 Rapid Algorithm Band Transmittance Model

The rapid transmittance algorithm used to compute band averaged transmittances as a function of temperature, moisture, and ozone profile is a refinement of the approach originally used by Susskind et al (1983) to model channel transmittances for the HIRS2 instrument of TIROS-N. Analogous methodology for modeling the TOVS channel transmittance is used in analyzing the TOVS data in the Pathfinder Path A data set (Susskind et al 1997).

As in Susskind et al (1983), we select a form for band i averaged transmittances $\tau_i(P)$, which reflects the behavior of monochromatic transmittances $\tau_\nu(P)$, where $\tau_\nu(P)$ represents the transmittance from pressure P to the boundary pressure P_b, and P_b is the top of the

atmosphere in the case of upwelling radiation, and the surface in the case of downwelling radiation. The monochromatic expressions are exact and given by the two basic relations :

$$\tau_v(P_j) = \prod_{j=1}^{J} \tau_v(P_j, P_{j-1}), \qquad 2.9$$

where $\tau_v(P_j, P_{j-1})$ is the transmittance in a layer between P_j and P_{j-1}, and

$$\tau_v(P_j, P_{j-1}) = \tau_v^f(P_j, P_{j-1})\, \tau_v^w(P_j, P_{j-1})\, \tau_v^o(P_j, P_{j-1})\, \tau_v^{wc}(P_j, P_{j-1})\, \tau_v^{nc}(P_j, P_{j-1}) \qquad 2.10$$

where τ^f, τ^w, and τ^o represent transmittance of gases with fixed distribution, water vapor, and ozone respectively, and τ^{wc} and τ^{nc} represent transmittances resulting from water vapor continuum and nitrogen continuum absorption.

Our goal is to model the band averaged transmittance $\tau_i(P)$ to be used in Equation 2.5 for the computation of fluxes as a function of atmospheric temperature and constituent profile. It is convenient to use equations of the form of equations 2.9 and 2.10. But equations of the form of 2.9 and 2.10 do not hold for band averaged transmittances unless the transmittances under question are constant across the band, or the terms being multiplied are uncorrelated in frequency. We therefore define effective band i transmittances, $\bar{\tau}_i(P_j, P_{j-1})$, $\bar{\tau}_i(P_j, P_{j-1})\, \bar{\tau}_i^w(P_j, P_{j-1})$, and $\bar{\tau}_i^o(P_j, P_{j-1})$, in a manner such that the analogous equations hold:

$$\tau_i(P) = \prod_{j=1}^{J} \bar{\tau}_i(P_j, P_{j-1}) \qquad 2.11$$

and

$$\bar{\tau}_i(P_j, P_{j-1}) = \bar{\tau}_i^f(P_j, P_{j-1})\, \bar{\tau}_i^w(P_j, P_{j-1})\, \bar{\tau}_i^o(P_j, P_{j-1}). \qquad 2.12$$

Note that continuum absorption varies only slowly with frequency in a band so the inclusion of band average values for those terms in equations of the form of 2.9 and 2.10 will not introduce an appreciable error in the use of analogous expressions for band averaged transmittances.

To ensure the form of Equations 2.11 and 2.12, we define

$$\bar{\tau}_i\left(P_j, P_{j-1}\right) \equiv \tau_i^{fwo}\left(P_j\right) / \tau_i^{fwo}\left(P_{j-1}\right) \qquad 2.13$$

$$\bar{\tau}_i^f\left(P_j, P_{j-1}\right) \equiv \tau_i^f\left(P_j\right) / \tau_i^f\left(P_{j-1}\right) \qquad 2.14$$

$$\bar{\tau}_i^w\left(P_j, P_{j-1}\right) \equiv \frac{\tau_i^{fw}\left(P_j\right)}{\tau_i^f\left(P_j\right)} \left(\frac{\tau_i^{fw}\left(P_{j-1}\right)}{\tau_i^f\left(P_{j-1}\right)} \right)^{-1} \qquad 2.15$$

and

$$\bar{\tau}_i^o\left(P_j, P_{j-1}\right) \equiv \frac{\tau_i^{fwo}\left(P_j\right)}{\tau_i^{fw}\left(P_j\right)} \left(\frac{\tau_i^{fwo}\left(P_{j-1}\right)}{\tau_i^{fw}\left(P_{j-1}\right)} \right)^{-1} , \qquad 2.16$$

where the terms $\tau_i^{fwo}\left(P_j\right), \tau_i^{fw}\left(P_j\right)$, and $\tau_i^f\left(P_j\right)$ refer to band averaged transmittances, from pressure P_j to P_b, due to absorption by fixed gases, water, and ozone; fixed gases and water; and fixed gases alone; respectively.

The goal of the rapid algorithm is now to model $\bar{\tau}_i^f\left(P_j, P_{j-1}\right)$, $\bar{\tau}_i^w\left(P_j, P_{j-1}\right)$, and $\bar{\tau}_i^o\left(P_j, P_{j-1}\right)$ in terms of the temperature, moisture, and ozone profile of the atmosphere. In the case of monochromatic transmittances, these terms would depend only on the atmospheric parameters in the layer P_j, P_{j-1}. For band averaged effective transmittances, all forms of $\bar{\tau}_i\left(P_j, P_{j-1}\right)$ also depend on conditions between P_{j-1} and the boundary pressure P_b. The coefficients of the model are generated based on a set of line by line calculations, in which all terms in Equations 2.13-2.16 are computed for the ensemble of 22 profiles, each done at the appropriate zenith angle θ_i for band i (as described in Section 2.2).

The form of the rapid algorithm parameterizes $\bar{\tau}_i^f\left(P_j, P_{j-1}\right)$, $\bar{\tau}_i^w\left(P_j, P_{j-1}\right)$, and $\bar{\tau}_i^o\left(P_j, P_{j-1}\right)$ in terms of the mean temperature in layer P_j, P_{j-1}, the column density of water vapor and the column density of O_3 in the layer P_j, P_{j-1}, and accounts for the temperature-water vapor-ozone profile between P_{j-1} and P_b. Appropriate coefficients are generated for both OLR transmittances, for which $P_b = 0$ mb, and DSF transmittances, for which $P_b = 1050$ mb. Note also that the definition of $\bar{\tau}_i\left(P_j, P_{j-1}\right)$ is different for OLR and DSF. For all terms, we parameterize the effective layer optical depth, $\ln \bar{\tau}_i\left(P_j, P_{j-1}\right)$, as a linear combination of the variables.

In the case of fixed gas absorption, the transmittances depend only on the temperature profile. We model

$$\ln \bar{\tau}_i^f\left(P_j, P_{j-1}\right) = A_{i,j} + B_{i,j}\left(\Delta T_{j,j-1}\right) + C_{i,j}\left(\Delta T_{j,j-1}\right)^2 + D_{i,j}\Delta T_{ABOVE_{j-1}} \qquad 2.17$$

$\Delta T_{j,j-1}$ in Equation 2.17 is given by the difference between the profile temperature in the layer between P_j and P_{j-1}, and that of a standard temperature profile $T^0_{j,j-1}$. $\Delta T_{ABOVE_{j-1}}$ in Equation 2.17 is a weighted difference of the temperature profile above (below for downward flux) P_{j-1} from that of a standard temperature profile

$$\Delta T_{ABOVE_{j-1}} = \sum_{k=1}^{j-1} \frac{\Delta T_{k,k-1}\left(\bar{\tau}_i^f\left(P_k\right) - \bar{\tau}_i^f\left(P_{k-1}\right)\right)}{1 - \bar{\tau}_i^f\left(P_{k-1}\right)} \qquad 2.18$$

which weights layers above (below for DSF) P_{j-1} according to their importance in the radiance integral. For each band, and layer, we have 22 linear equations to determine the four coefficients. The coefficient D_{ij} is set equal to zero for j=1, and for cases in which $\bar{\tau}_j^f\left(P_j\right)$ is greater than 0.99, indicating that the levels above j do not contribute significantly to the radiance.

For the water vapor and ozone, we parameterize the effective absorption coefficients in terms of the water vapor profile and ozone profile respectively. The model at this time ignores the temperature dependence of the water vapor and ozone line absorption. As in the case of the the fixed gas transmittance (equation 2.17), the profile is referenced to the standard water vapor and ozone profiles $u^0_{wj,j-1}$ and $u^0_{oj,j-1}$ according to $r_j = \left(\frac{u_{j,j-1}}{u^0_{j,j-1}}\right)$, where $u_{j,j-1}$ is the column layer density in the given profile.

For water vapor we write

$$\ln \bar{\tau}_i^w\left(P_j, P_{j-1}\right) = E_{i,j}\, r_{w,j}^{1/2} + F_{i,j}\, r_{w,j} + G_{i,j}\, r_{w,j}^2 + H_{i,j}\, r_{wABOVE,j-1} \qquad 2.19$$

where $r_{wABOVE,j-1}$ is a weighted estimate of the effect of the water vapor ratio above (below for DSF) P_{j-1}, given by

$$r_{wABOVE,j-1} = \frac{\ln \bar{\tau}_{iw}\left(P_{j-1}\right)}{\ln \bar{\tau}^{0}_{iw}\left(P_{j-1}\right)} \qquad 2.20$$

where $\bar{\tau}^{0}_{iw}\left(P_{j-1}\right)$ is the effective water vapor transmittance for the standard profile. As with temperature, we have 22 equations to determine four unknowns in each layer. $H_{i,j}$ is set equal to zero if j = 1 or $\bar{\tau}^{0}_{iw}\left(P_{j-1}\right) > 0.99$. The ozone algorithm is identical in form to the water vapor algorithm, with coefficients I, J, K, and L for band i and layer j, j-1, except that coefficient L multiplies a slightly different term for $r_{o\,ABOVE,j-1}$ given by

$$r_{o\,ABOVE,j-1} = \left[\frac{\ln \bar{\tau}_{io}\left(P_{j-1}\right)}{\ln \tau^{0}_{io}\left(P_{j-1}\right)}\right]^{1/2}, \qquad 2.21$$

The form of this term for ozone was found to fit the line by line calculations better than the form used for water.

Based on the parameterized transmittances, clear sky OLR and DSF are obtained according to Equation 2.5, with analogous equations for cloudy OLR and DSF. In the following section, the accuracy of the model calculations of OLR and DSF are presented by comparing them with the line by line calculations carried out by us and also with those provided by the ICRCCM results.

3.0 Accuracy of the Longwave Fluxes

3.1 Comparison with line by line Calculations

Given the accuracy of the line by line calculations, the calculations of OLR and DSF are based on two approximations: use of the effective zenith angle for each band to account for angular integration; and use of the rapid algorithm for band transmittance, together with the evaluation of the Planck function for each band at its central frequency, to account for frequency integration. If both approximations were perfect, band fluxes would agree exactly with those obtained from line by line calculations for the same profiles. It is therefore necessary to assess how well the model calculations compare with the line by line calculations. This comparison should be done for both clear and cloudy conditions. For the cloudy comparison, a cloud with emissivity=1 is placed at the 500 mb level in each of the 22 profiles. OLR and DSF are then calculated for clear and cloudy conditions by the line by line method and by using the model described in the previous section.

Results of the line by line and the model calculations of OLR and DSF for the clear-sky and cloudy cases for the 22 profiles are shown in Figure 4. Corresponding means and standard deviations are given in Tables 2a and 2b for both total OLR and its spectral components, and in Tables 2c and 2d for DSF. As shown in Figure 4, our model calculations of OLR (left panel) and DSF (right panel) for clear-sky and cloudy conditions agree well with the corresponding line by line calculations. As shown in the Tables 2a, 2b, 2c, and 2d, agreement for all the spectral components is also good. The mean differences between the line by line and the model calculations of total OLR under clear conditions is 0.26 $W \cdot m^{-2}$ and the standard deviation is 1.31 $W \cdot m^{-2}$. For the cloudy conditions, the mean difference of total OLR is 0.44 $W \cdot m^{-2}$ and the standard deviation is 1.89 $W \cdot m^{-2}$. For total DSF, the mean differences are -0.71 $W \cdot m^{-2}$ and -0.3 $W \cdot m^{-2}$ for clear and cloudy conditions respectively. Corresponding standard deviations of DSF are 0.56 $W \cdot m^{-2}$ and 0.18 $W \cdot m^{-2}$. These errors result from a combination of errors due to errors in the frequency and angle integral approximations, as well as the band transmittance algorithm error.

As described in the previous section, we used the band-dependent effective zenith angles to approximate the angular integration required to calculate OLR and DSF. The conventional diffusivity approximation uses a frequency-independent effective zenith angle of 52.96°. Band coefficients are found which represent nadir transmittances (effective zenith angle of 0°) and when used in the calculations the nadir optical path is scaled by the factor 1.66 = secant (52.96°). As described in Section 2.3, the model we use to calculate the band transmittance was originally developed and used for HIRS channel transmittances. In the model, layer band transmittances for water vapor and ozone are parameterized as a non-linear function of the ratio of layer column density to the column density of the appropriate gas in the reference profile. Therefore, in the context of our model, the conventional diffusivity approximation, in terms of scaling the optical path, is not directly applicable. Instead, line by line calculations for each band are carried out at the appropriate effective zenith angles to obtain the band transmittances.

To examine different approaches of angular integration, we carried out two additional sets of OLR and DSF calculations. In the first case, the band dependence of the effective zenith angle is ignored, and the monochromatic transmittances are calculated at a constant zenith angle of 52.96° and then averaged for use in the parameterization of the band transmittances. The second case uses a different approach, in which monochromatic transmittances for a given profile are first integrated over all zenith angles using Gaussian quadrature and then averaged to obtain the band transmittances. In both these cases, appropriate rapid algorithm model coefficients based on the line by line calculations, as described in Section 2.3, are generated. Total flux values computed by using each of these

approaches, along with those obtained from line by line calculations and our own model calculations (as shown in Table 2a and 2c) are given in Table 3. As shown in Table 3, in the first additional case (column C), the mean difference of OLR from line by line calculations is -0.61 $W \cdot m^{-2}$ (standard deviation of 1.63 $W \cdot m^{-2}$) and that of DSF is 0.92 $W \cdot m^{-2}$ (standard deviation 0.57 $W \cdot m^{-2}$). The mean total OLR in the second case (column D) differs by -0.39 $W \cdot m^{-2}$ (standard deviation is 1.36 $W \cdot m^{-2}$) and DSF differs by 0.86 $W \cdot m^{-2}$ (standard deviation is 0.62 $W \cdot m^{-2}$) compared to the line by line calculations. These values are marginally poorer than those obtained by using our model (column B in Table 3). Calculation C in Table 3 shows that use of a frequency-dependent value of the zenith angle itself is not very critical. Calculation D in Table 3 shows that integrating monochromatic transmittances over angles and using these to obtain a rapid algorithm is almost as good as finding band transmittances at effective angles which match the band radiative fluxes.

In addition to the above cases, we have carried out a calculation in which transmittances at nadir are averaged to get band transmittances, and then the rapid algorithm coefficients are found. When calculating OLR and DSF, these band transmittances are then raised to the factor 1.66. As shown in column E of Table 3, clearly, this approach is very poor and introduces large biases in OLR and DSF. The bias is negative (-14.24 $W \cdot m^{-2}$) in OLR with a standard deviation of 2.78 $W \cdot m^{-2}$, and positive (8.03 $W \cdot m^{-2}$) in DSF with a standard deviation of 3.40 $W \cdot m^{-2}$, suggesting that absorption is overestimated in both calculations. This is expected because $\overline{\tau_\nu^{\sec\theta}}$ is always greater than $\overline{\tau_\nu}^{\sec\theta}$, where the bar represents frequency average, except for the special case in which τ is independent of ν in the band. This last calculation of raising the band transmittances to 1.66, although not commonly used in band models, is carried out to indicate what would be the magnitude of error if the diffusivity approximation is mistakenly applied directly to band transmittances instead of optical paths (effective absorber amount). From the results presented in Table 3, it appears that if the angular integration is carried out for the monochromatic transmittances, and the band parameters are found from the angle-integrated transmittances, the method of exact angular integration is not critical. But, in the context of our band model, which does not directly use optical mass, the approach we have used is correct and accurate. The benefits of this approach perhaps would be more evident if used in calculations of outgoing flux from narrow spectral bands.

3.2 Comparison with the ICRCCM Results

In the previous section, we have shown that our model-calculations agree very well with our line by line calculations for clear-sky and cloudy conditions. We now compare our model calculations of OLR and DSF with those of ICRCCM results for clear-sky and cloudy conditions. We have used the standard atmospheric profiles of temperature, water vapor, and

ozone provided by the ICRCCM committee for tropical, mid-latitude summer and winter, subarctic summer and winter conditions as compiled by McClatchey et al. (1972). For clear-sky conditions, we have calculated OLR and DSF using our model for cases 25, 27, 29, 31, and 33 of the ICRCCM tests (see Table 3 of Ellingson et al., 1991). Calculations of three line by line models, selected from more than 30 different models included in the ICRCCM, have been chosen for the comparison with our model calculations. The results of the comparison are shown in Table 4a. As shown in Table 4a, our band model calculations of OLR and DSF are within the range of 0.3% to 1.4% compared to the line by line calculations, and compare with the other line by line calculations as closely as they do to themselves. The major differences result from different assumptions about line and continuum absorption characteristics.

For the cloudy case, we have used the mid-latitude summer profile and have carried out four different calculations of OLR and DSF as provided by the ICRCCM test cases corresponding to different cloud opacities. It is important to note that in the Pathfinder Path A calculations of OLR and DSF, we use the effective cloud amount which is a product of cloud emissivity and cloud fraction as determined from the TOVS measurements (Susskind et al., 1987). Therefore, we do not have to explicitly parameterize cloud emissivity in the model for our OLR and DSF calculations. However, to test our model, we have parameterized cloud emissivity as a function of liquid water path and effective cloud-drop size following Paltridge and Platt (1981), Stephens (1978), and Mehta and Smith (1997). The model calculations carried out using this parameterization are presented in Table 4b along with the ICRCCM results. For these cases, line by line calculations from ICRCCM were not available. Therefore, the ICRCCM results are presented in terms of mean, standard deviation, and range of OLR and DSF based on the different models (Table 11 in Ellingson et al., 1991) which were used in the ICRCCM comparison. We find that our OLR calculations are within 1% and DSF are within 0.6% of the ICRCCM means for these cases.

4.0 Summary

in this report, the radiative transfer model used to calculate OLR and DSF from the TOVS Pathfinder Path A retrieval products has been described. The model is computationally efficient and is being used to calculate global, twice-daily per satellite, multi-year OLR and DSF using the TOVS Pathfinder Path A retrievals, which include surface skin temperature, atmospheric temperature, moisture, and ozone profiles, cloud top pressure and temperature, and effective cloud fraction $\alpha\varepsilon$ (Susskind et al., 1997).

We have derived band-dependent effective zenith angles which are used for the angular integration of radiances in the model. These angles are used to calculate monochromatic transmittances at the appropriate angle which are then averaged to find band transmittances.

This is different from the conventional diffusivity approximation in which band transmittances as a function of optical path are found at nadir and the optical path of absorbers are scaled by the secant of a frequency-independent angle of 52.96°. The form of the rapid transmittance algorithm used for modeling the band transmittance is accurate for modeling wide band transmittances (100 to 300 cm-1) as used in the present study, as the model calculations differ by less than 0.2% from our line by line calculations. Our results are also within 1% range of the results provided by ICRCCM for clear-sky and cloudy conditions, with some of the differences from ICRCCM resulting from effects of different assumptions of line and continuum absorption characteristics.

As shown by Mehta and Susskind (1999), the OLR and COLR derived from TOVS Path A are in excellent agreement with the ERBE measurements. We intend to validate the DSF with available measurements and will report the results elsewhere. The TOVS Pathfinder Path A OLR data are currently available for 14 years (1985 to 1998) and will be extended to cover the period between 1979 to 1998 in near future.

More information about the Goddard TOVS Pathfinder Path A data set is available from : **http://faster.gsfc.nasa.gov/srt.html**

References

Barkstrom, B., Earth Radiation Budget Experiment (ERBE) archival and April 1985 results. *Bull. Amer. Meteor. Soc.* 70, 1254-1262, 1989 .

Briegleb, B. P., Longwave band model for thermal radiation in climate studies. *J. of Geophys. Res.*, 97, 11475-11485, 1992.

Chou, M. D., and L. Kouvaris, Calculations on transmission function in the IR CO_2 and O_3 bands. *J. Geophys. Res.*, 96, 9003-9012, 1991.

Darnell, W. L., W. F. Staylor, S. K. Gupta, N. A. Ritchey, and A. C. Wilber, Seasonal variations of surface radiation budget derived from international satellite cloud climatology project C1 data. *J. of Geophys. Res.*, 97, 15741-15760, 1992.

Ellingson, R. G., H. L. Lee, and D. Yanuk, A. Gruber, Validation of a technique for estimating outgoing longwave radiation from HIRS radiance observations. *J. Atmos. Oceanic Technol.*, 11, 357-365, 1994.

Ellingson, R. G., J. Ellis, and S. Fels, The intercomparison of radiation codes used in climate models: Longwave results. *J. Geophys. Res.*, 96, 8929-8953, 1991.

Elsasser, W. M., Heat transfer by infrared radiation in the atmosphere. *Harvard Meteorol. Stud. 6*, Harvard University Press, Cambridge, Mass., 1942.

Gruber, A., and A. F. Krueger, The status of the NOAA outgoing longwave radiation data set. *Bull Am. Meteorol. Soc.*, 65,958-962, 1984.

Gupta, S. K., W. L. Darnell, A. C. Wilber, A parameterization for longwave surface radiation from satellite date: Recent improvements. *J. App. Meteor.*, 31, 1361-1367, 1992.

Goody, R. M. and Y. L. Yung, Atmospheric radiation : Theoretical basis second edition, *Oxford University Press*, 519 pp, 1989.

Jacobowitz, H., H.V. Soule, H.L.Kyle, F.B.House, and the ERB Nimbus 7 Experiment Team, The Earth Radiation Budget (ERB) experiment: an overview, *J.Geophys. Res.*, 89, 5021-5038, 1984.

Kyle, H. L., J.R. Hickey, P. E. Ardanuy, H. Jacobowitz, A. Arking, G.G. Campbell, F.B. House, R. Maschhoff, G.L. Smith, L.L. Stowe, and T. Vonder Haar, The Nimbus Earth Radiation Budget (ERB) Experiment: 1975-1992, *Bull. Am. Meteorol. Soc., 74*, 815-830., 1993.

Lacis, A., and V. Oinas, A description of the correlation k-distribution method for modeling nongray gaseous absorption, thermal emission, and multiple scattering in vertically inhomogeneous atmospheres. *J. Geophys. Res.*, 96, 9027-9063, 1991.

McClatchey, R. A., R. W. Fenn, J.E.A.Selby, F. E. Volz, and J.S. Garing, Optical properties of the atmosphere (Third Edition). *Environmental Research Papers, No. 411, AFCRL, Bedford, MA,* 108 pp., 1972.

Mehta, A. V., and J. Susskind, Outgoing longwave radiation from the TOVS Pathfinder Path A data set. *o J. of Geophys. Res.,* 104,12193-12212 1999

Mehta, A. V., and E. A. Smith, Variability of radiative cooling during the Asian summer monsoon and its influence on intraseasonal waves. *J. Atmos. Sci.* , 54, 941-966, 1997.

Paltridge, G. W., and C. M. R. Platt, Aircraft measurements of solar and infrared radiation and the microphysics of cirrus clouds. *Quart. J. Roy. meteor. Soc,,* 107, 367-380, 1981.

Ramanathan, V., Scientific use of surface radiation budget data for climate studies. Surface Radiation Budget for Climate Applications. . *NASA Tech. Rep.*, RP-1169, 58-86, J. T. Suttles and G. Ohring editors, 1986.

Stephens, G. L., Review : The parameterizations of radiation for numerical weather prediction and climate models. *Mon. Wea. Rev.*, 112, 826-867, 1984.

Stephens, G. L., Radiation profiles in extended water clouds, II Parameterization schemes. *J. atmos. Sci.*, 35, 2123-2132, 1978.

Susskind, J., P. Piraino, L. Rokke, L. Iredell, and A. V. Mehta, Characteristics of the TOVS Pathfinder Path A data set. *Bull. of Amer. Meteorol. Soc. 78*, 1449-1472. 1997.

Susskind, J., J. Rosenfield, and D. Reuter, An accurate radiative transfer model for use in the direct physical inversion of HIRS2 and MSU temperature sounding data. *J. Geophys. Res.*, 88, 8550-8568, 1983.

Susskind, J., D. Reuter, and M. T. Chahine, Cloud fields retrieved from HIRS2/MSU data. *J. Geophys Res., 92D,* 4035-4050, 1987.

Susskind, J., and J. E. Searl., Synthetic atmospheric transmittance spectra near 15 μm and 4.3 μm. *J. Quant. Spectr. Rad. Trans.*, 19, 195-215, 1978.

Wu, M. C., and J. Susskind, Outgoing long-wave radiation from HIRS2/MSU soundings. *J. of Geophys. Res.* 95, 7579-7602, 1990.

List of Figures

List of Tables

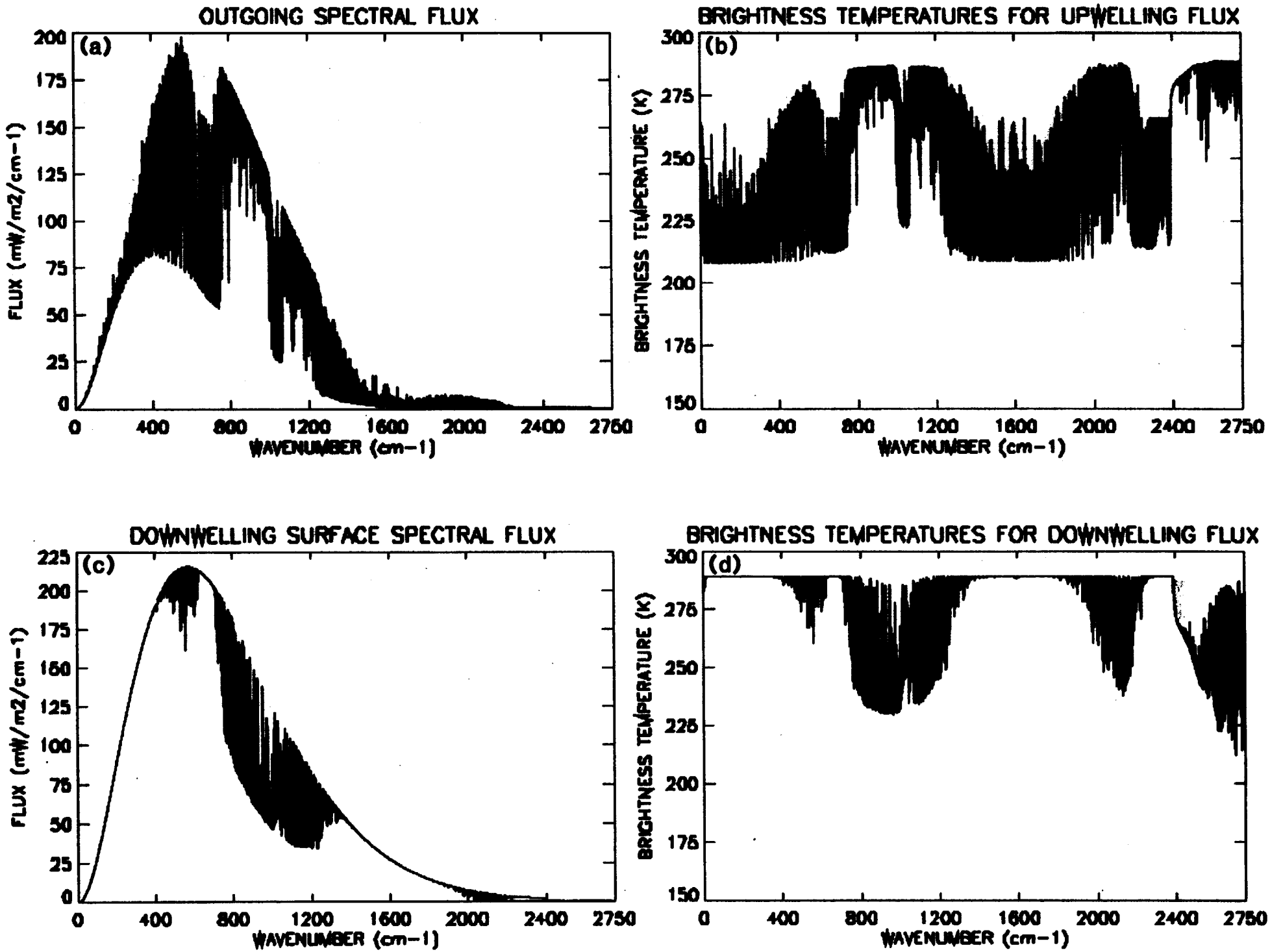
OUTGOING SPECTRAL FLUX
(a)
FLUX (mW/m2/cm-1)
WAVENUMBER (cm-1)
BRIGHTNESS TEMPERATURES FOR UPWELLING FLUX
(b)
BRIGHTNESS TEMPERATURE (K)
WAVENUMBER (cm-1)
DOWNWELLING SURFACE SPECTRAL FLUX
(c)
FLUX (mW/m2/cm-1)
WAVENUMBER (cm-1)
BRIGHTNESS TEMPERATURES FOR DOWNWELLING FLUX
(d)
BRIGHTNESS TEMPERATURE (K)
WAVENUMBER (cm-1)

Figure 1

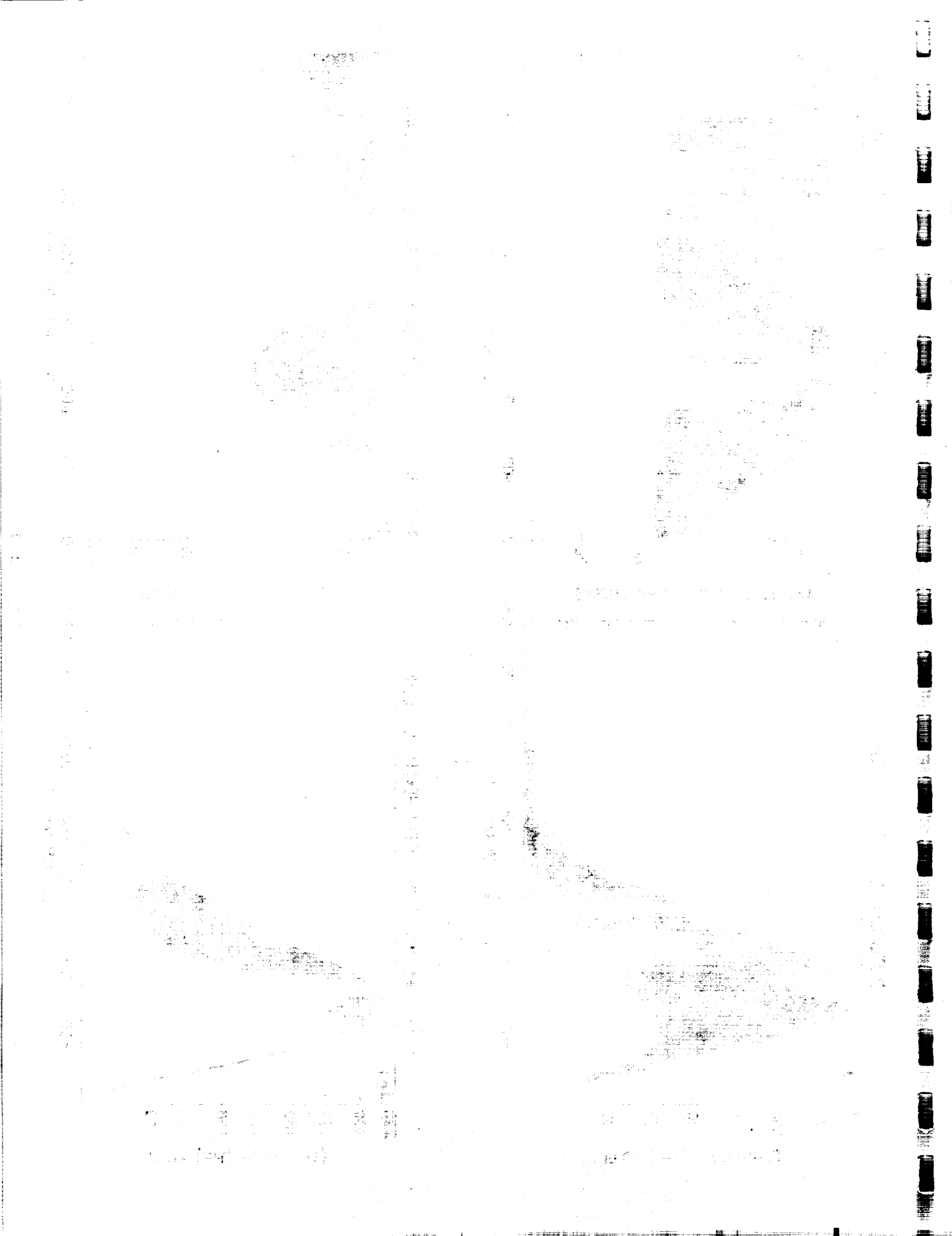

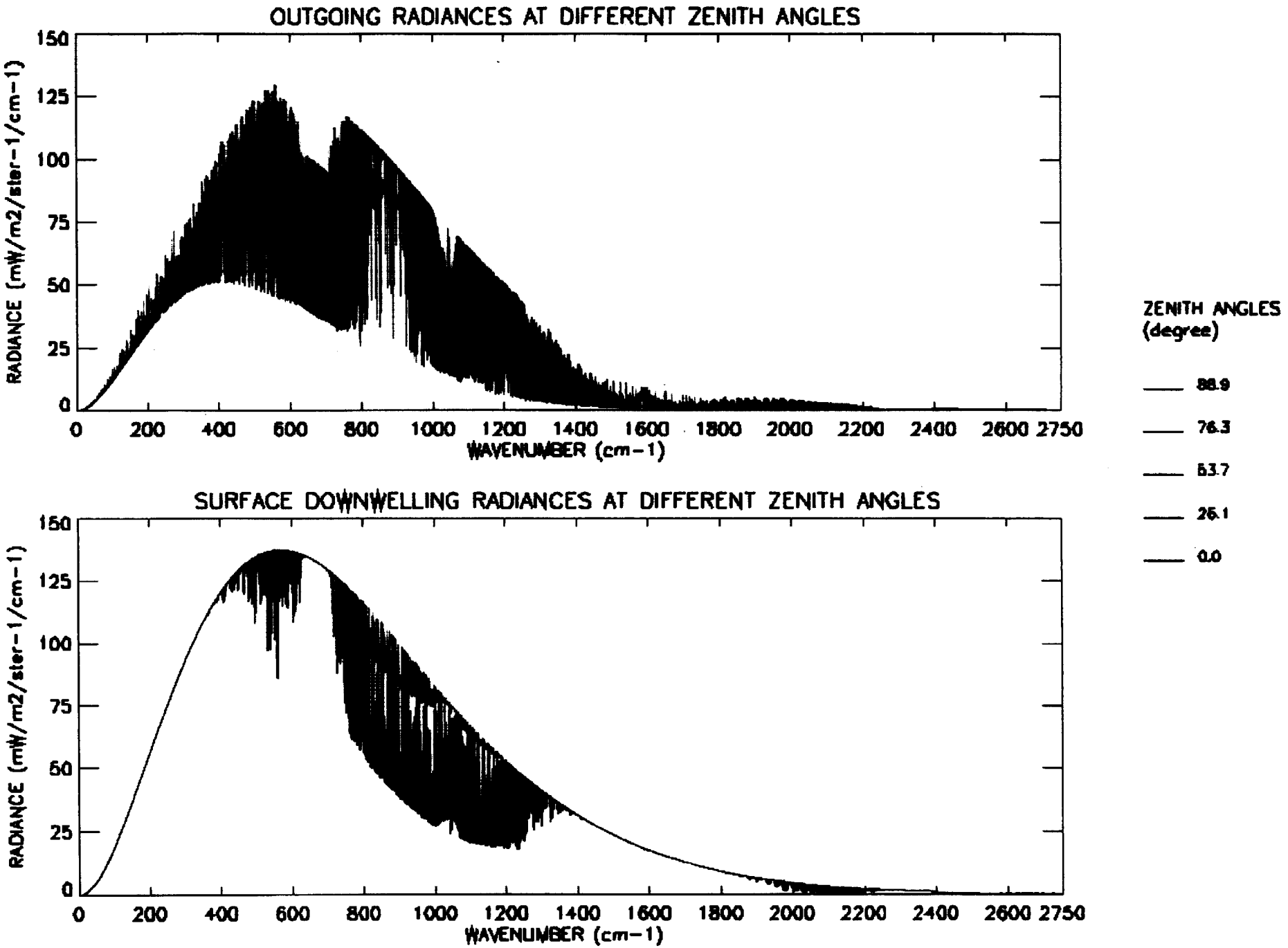
OUTGOING RADIANCES AT DIFFERENT ZENITH ANGLES
RADIANCE (mW/m2/ster-1/cm-1)
WAVENUMBER (cm-1)
SURFACE DOWNWELLING RADIANCES AT DIFFERENT ZENITH ANGLES
RADIANCE (mW/m2/ster-1/cm-1)
WAVENUMBER (cm-1)
ZENITH ANGLES (degree)
88.9
76.3
53.7
25.1
0.0

Figure 2

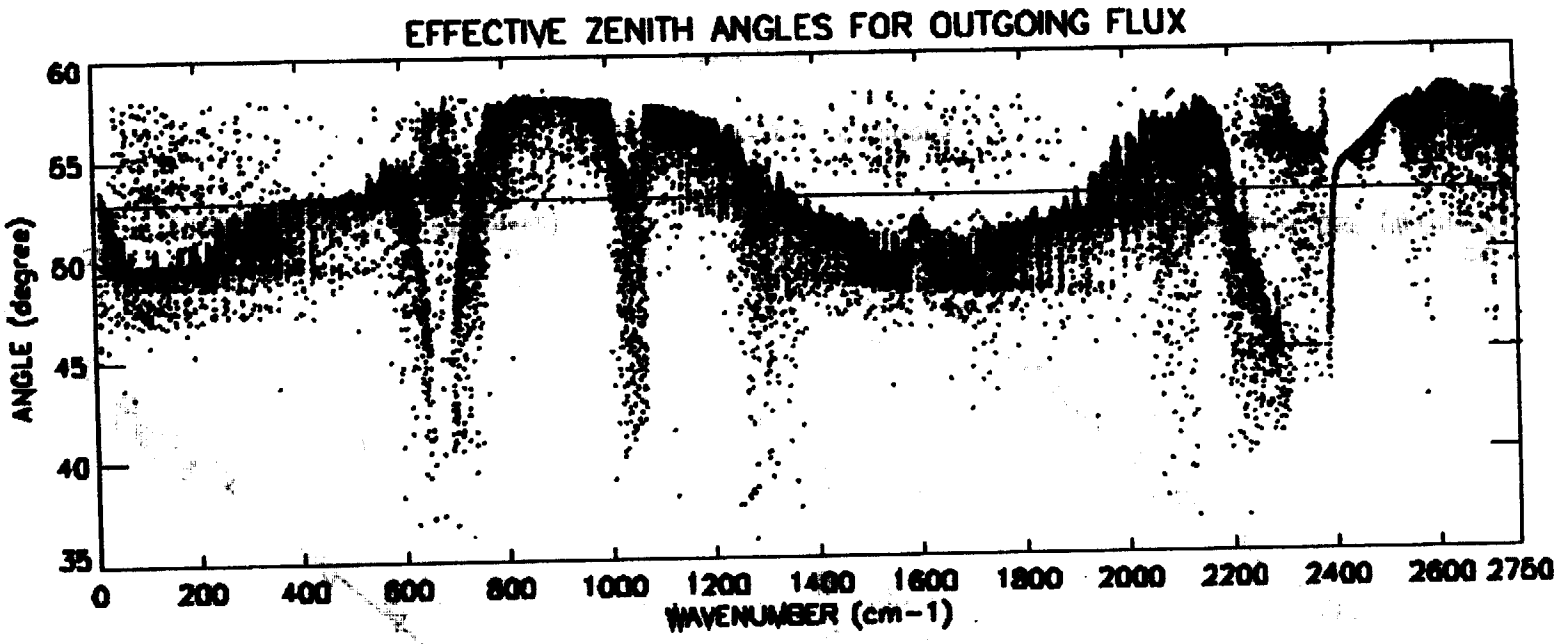
EFFECTIVE ZENITH ANGLES FOR OUTGOING FLUX
ANGLE (degree)
60
55
50
45
40
35
0
200
400
600
800
1000
1200
1400
1600
1800
2000
2200
2400
2600
2750
WAVENUMBER (cm-1)

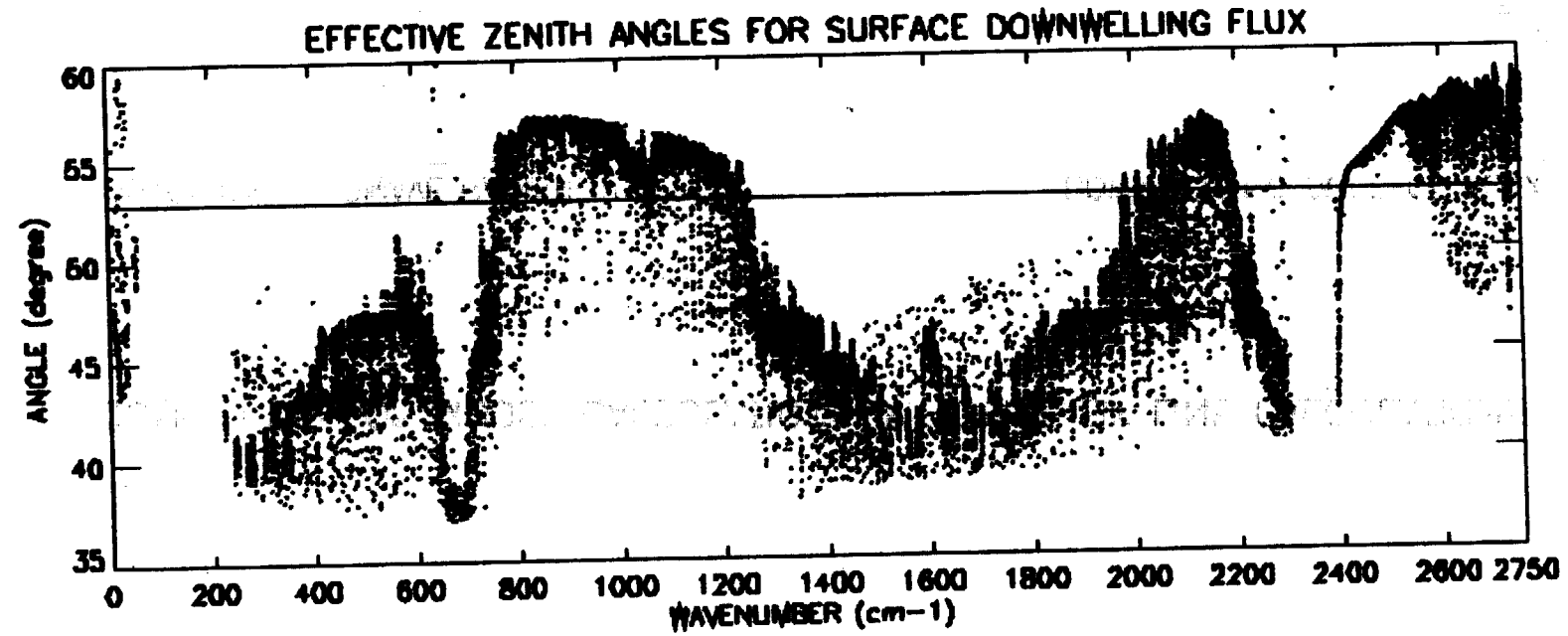
EFFECTIVE ZENITH ANGLES FOR SURFACE DOWNWELLING FLUX
ANGLE (degree)
60
55
50
45
40
35
0
200
400
600
800
1000
1200
1400
1600
1800
2000
2200
2400
2600
2750
WAVENUMBER (cm-1)

Figure 3

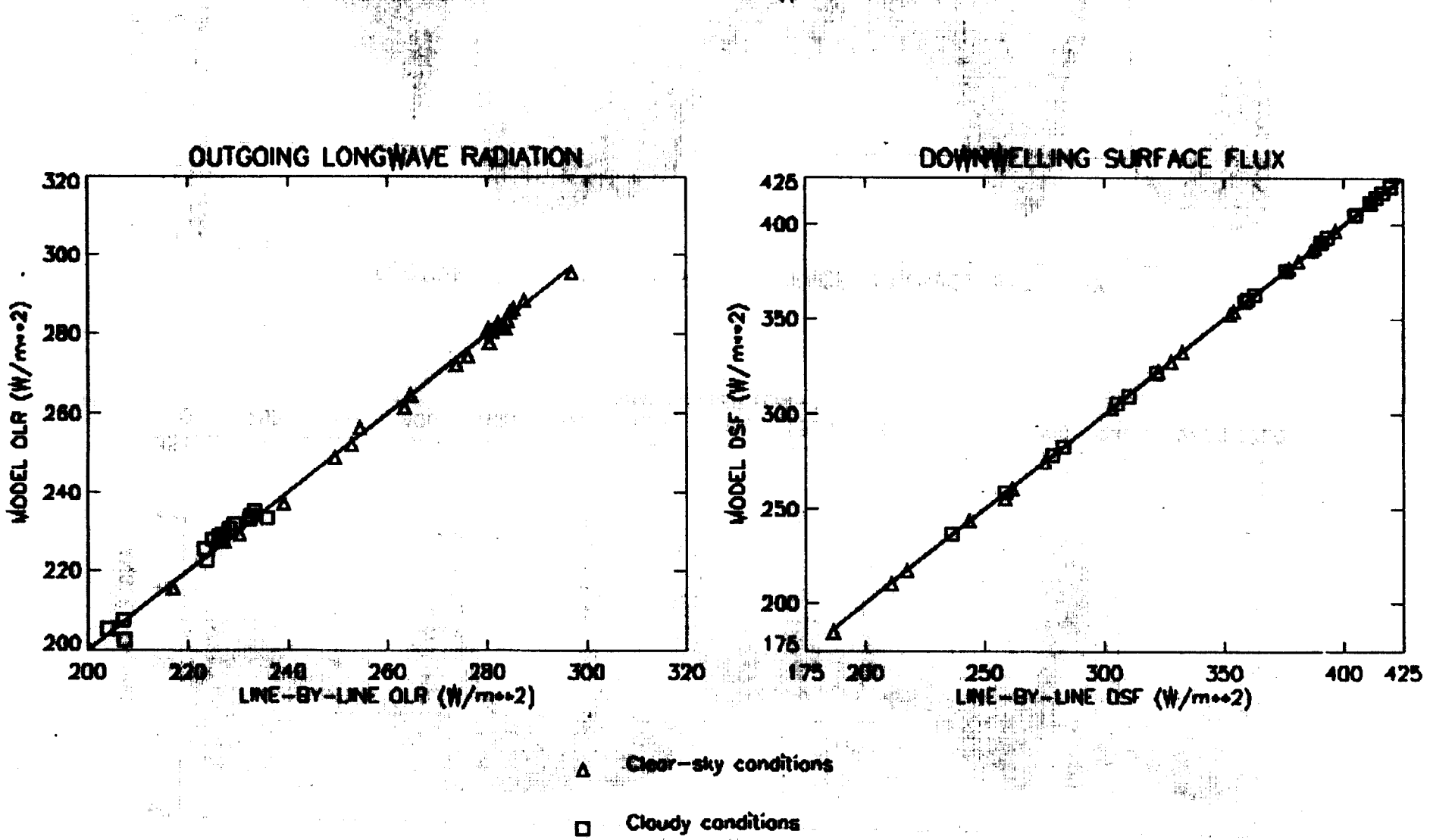
COMPARISON OF MODEL CALCULATIONS WITH LINE BY LINE CALCULATIONS
OUTGOING LONGWAVE RADIATION
MODEL OLR (W/m**2)
LINE-BY-LINE OLR (W/m**2)
320
300
280
260
240
220
200
200
220
240
260
280
300
320
DOWNWELLING SURFACE FLUX
MODEL DSF (W/m**2)
LINE-BY-LINE DSF (W/m**2)
425
400
350
300
250
200
175
175
200
250
300
350
400
425
Clear-sky conditions
Cloudy conditions

Figure 4

Table 1a

Equivalent Zenith Angles for OLR

Band (cm^{-1})	Equivalent Zenith Angle (St.Dev) degree θ_e ($\Delta\theta_e$)	sec (θ_e)
2 - 150	50.36 (0.59)	1.57
150 - 250	50.64 (0.65)	1.58
250 - 350	51.62 (0.53)	1.61
350 - 500	52.57 (0.48)	1.65
500 - 650	52.53 (0.37)	1.64
650 - 800	52.94 (0.09)	1.66
800 - 950	55.86 (0.78)	1.78
950 - 1100	53.08 (0.29)	1.67
1100 - 1250	55.21 (0.26)	1.75
1250 - 1500	51.64 (0.33)	1.61
1500 - 1800	50.36 (0.33)	1.57
1800 - 2100	52.51 (0.41)	1.64
2100 - 2400	52.74 (0.12)	1.66
2400 - 2750	55.08 (0.14)	1.69

Table 1b

Equivalent Zenith Angles for DSF

Band (cm^{-1})	Equivalent Zenith Angle (St.Dev) degree θ_e ($\Delta\theta_e$)	sec (θ_e)
2 - 100	44.99 (0.36)	1.41
100 - 250	44.54 (0.28)	1.40
250 - 350	44.20 (0.33)	1.39
350 - 500	43.79 (1.57)	1.38
500 - 650	46.04 (2.24)	1.44
650 - 800	52.12 (0.15)	1.63
800 - 950	55.71 (0.23)	1.77
950 - 1100	54.82 (0.19)	1.74
1100 - 1250	53.92 (0.56)	1.70
1250 - 1500	47.45 (1.14)	1.48
1500 - 1800	42.88 (0.74)	1.37
1800 - 2100	50.57 (0.58)	1.57
2100 - 2400	52.38 (0.17)	1.64
2400 - 2750	54.85 (0.07)	1.74

Table 2a

Comparison of Model Outgoing Longwave Radiation with Line-by-Line Calculations
Clear-sky Condition

Band	Line-by-line	Model	Model - Line by line
	Mean (St. Dev.)	Mean (St. Dev.)	Mean Difference (St. Dev.)
Cm^{-1}	$W \cdot m^{-2}$	$W \cdot m^{-2}$	$W \cdot m^{-2}$
2-150	4.23 (0.17)	4.16 (0.15)	-0.07 (0.05)
150-250	10.94 (0.47)	10.98 (0.53)	0.04 (0.07)
250-350	18.41 (0.61)	18.46 (0.74)	0.06 (0.18)
350-500	42.45 (1.78)	42.60 (1.82)	0.15 (0.48)
500-650	42.93 (2.12)	43.17 (2.19)	0.23 (0.16)
650-800	34.56 (2.33)	34.69 (2.31)	0.13 (0.16)
800-950	46.53 (5.75)	46.68 (5.80)	0.15 (0.06)
950-1100	27.31 (4.92)	26.99 (4.88)	-0.32 (0.19)
1100-1250	23.00 (3.74)	22.90 (3.71)	-0.11 (0.07)
1250-1500	10.46 (1.30)	10.61 (1.35)	0.15 (0.34)
1500-1800	2.33 (0.32)	2.27 (0.39)	-0.06 (0.13)
1800-2100	2.61 (0.53)	2.70 (0.57)	0.09 (0.08)
2100-2400	0.74 (0.21)	0.58 (0.16)	-0.16 (0.06)
2400-2750	0.58 (0.21)	0.56 (0.20)	-0.02 (0.01)
Total : 2-2750	267.11 (21.92)	267.37 (22.11)	0.26 (1.31)

Table 2b

Comparison of Model Outgoing Longwave Radiation with Line-by-Line Calculations
Cloudy Condition : 100 % cloud cover with top at 500 mb, cloud emissivity = 1.0

Band	Line-by-line	Model	Model - line by line
	Mean (St. Dev.)	Mean (St. Dev.)	Mean Difference (St. Dev.)
Cm^{-1}	$W \cdot m^{-2}$	$W \cdot m^{-2}$	$W \cdot m^{-2}$
2-150	4.23 (0.17)	4.16 (0.15)	-0.07 (0.05)
150-250	10.94 (0.47)	10.98 (0.53)	0.04 (0.07)
250-350	18.31 (0.65)	18.39 (0.74)	0.08 (0.35)
350-500	39.63 (2.63)	39.53 (1.82)	-0.10 (1.26)
500-650	38.12 (3.12)	38.57 (2.19)	0.45 (0.11)
650-800	28.63(2.53)	28.88 (2.31)	0.25 (0.10)
800-950	29.79 (4.99)	29.82 (5.80)	0.03 (0.03)
950-1100	17.40 (3.47)	17.71 (4.88)	0.31 (0.07)
1100-1250	13.28 (2.88)	13.27 (3.71)	-0.01 (0.01)
1250-1500	8.32 (1.53)	7.95 (1.35)	-0.37 (0.21)
1500-1800	2.19 (0.36)	2.14 (0.39)	-0.05 (0.10)
1800-2100	1.46 (0.43)	1.43 (0.57)	-0.03 (0.03)
2100-2400	0.33 (0.10)	0.26 (0.16)	-0.07 (0.03)
2400-2750	0.16 (0.06)	0.14 (0.20)	-0.02 (0.01)
Total : 2-2750	212.79 (21.63)	213.23 (21.96)	0.44 (1.89)

Table 2c

Comparison of Model Downwelling Surface Longwave Radiation with Line-by-Line Calculations Clear-sky Condition

Band	Line-by-line	Model	Model - Line by line
	Mean (St. Dev.)	Mean (St. Dev.)	Mean Difference (St. Dev.)
Cm^{-1}	$W \cdot m^{-2}$	$W \cdot m^{-2}$	$W \cdot m^{-2}$
2-100	2.06 (0.09)	1.68 (0.07)	-0.38 (0.01)
100-250	21.72 (1.16)	21.63 (1.12)	-0.09 (0.04)
250-350	29.05 (1.94)	29.24 (1.94)	0.19 (0.00)
350-500	57.60 (5.97)	58.28 (6.14)	0.68 (0.21)
500-650	61.64 (9.54)	62.62 (9.51)	0.98 (0.15)
650-800	52.31 (10.60)	52.38 (11.22)	0.07 (0.63)
800-950	23.19 (13.53)	22.83 (13.56)	-0.36 (0.19)
950-1100	17.20 (7.97)	16.62 (7.76)	-0.58 (0.26)
1100-1250	14.21 (6.73)	14.04 (6.75)	-0.16 (0.11)
1250-1500	25.84 (6.26)	25.58 (6.24)	-0.26 (0.10)
1500-1800	14.44 (3.65)	14.00 (3.59)	-0.43 (0.06)
1800-2100	4.76 (1.65)	4.36 (1.61)	-0.41 (0.05)
2100-2400	1.38 (0.50)	1.44 (0.50)	0.06 (0.01)
2400-2750	0.16 (0.06)	0.13 (0.06)	-0.03 (0.01)
Total : 2-2750	325.53 (68.70)	324.83 (69.03)	-0.71 (0.56)

Table 2d

Comparison of Model Downwelling Surface Longwave Radiation with Line-by-Line Calculations
Cloudy Condition : 100 % cloud cover with base at 500 mb, cloud emissivity = 1.0

Band	Line-by-line	Model	Model - Line by line
	Mean (St. Dev.)	Mean (St. Dev.)	Mean Difference (St. Dev.)
Cm^{-1}	$W \cdot m^{-2}$	$W \cdot m^{-2}$	$W \cdot m^{-2}$
2-100	2.06 (0.09)	1.68 (0.07)	-0.38 (0.01)
100-250	21.72 (1.16)	21.63 (1.12)	-0.09 (0.04)
250-350	29.05 (1.94)	29.24 (1.94)	0.19 (0.00)
350-500	58.06 (5.22)	58.77 (5.27)	0.71 (0.05)
500-650	63.11 (7.66)	63.78 (7.77)	0.67 (0.12)
650-800	56.30 (8.65)	56.53 (8.82)	0.23 (0.18)
800-950	38.18 (9.52)	37.90 (9.43)	-0.28 (0.15)
950-1100	27.14 (7.21)	26.89 (7.16)	-0.25 (0.06)
1100-1250	20.15 (5.84)	20.07 (5.85)	-0.08 (0.05)
1250-1500	26.11 (6.09)	25.80 (6.07)	-0.31 (0.06)
1500-1800	14.44 (3.65)	14.00 (3.59)	-0.44 (0.06)
1800-2100	4.94 (1.63)	4.60 (1.59)	-0.34 (0.05)
2100-2400	1.51 (0.53)	1.56 (0.54)	0.05 (0.02)
2400-2750	0.27 (0.11)	0.28 (0.12)	0.01 (0.02)
Total : 2-2750	363.03 (58.98)	362.73 (59.01)	-0.30 (0.18)

Table 3

Comparison of OLR and DSF with different methods of angular integration

Band Total 2-2750 cm-1	A Mean (St. Dev.) $W \cdot m^{-2}$	B Mean (St. Dev.) $W \cdot m^{-2}$	C Mean (St. Dev.) $W \cdot m^{-2}$	D Mean (St. Dev.) $W \cdot m^{-2}$	E Mean (St. Dev.) $W \cdot m^{-2}$	B-A Mean (St. Dev.) $W \cdot m^{-2}$	C-A Mean (St. Dev.) $W \cdot m^{-2}$	D-A Mean (St. Dev.) $W \cdot m^{-2}$	E-A Mean (St. Dev.) $W \cdot m^{-2}$
OLR	267.11 (21.92)	267.37 (22.11)	266.57 (22.13)	266.71 (22.09)	252.86 (21.30)	0.26 (1.31)	-0.61 (1.63)	-0.39 (1.36)	-14.24 (2.78)
DSF	325.53 (68.70)	324.83 (69.03)	326.45 (68.49)	326.396 (68.92)	333.56 (65.53)	-0.71 (0.56)	0.92 (0.57)	0.86 (0.57)	8.03 (3.40)

A) Line-by-line calculations, B) Model calculations as shown in Table 2a and 2c, C) Monochromatic transmittances are found at 52.96° and then the model coefficients are found for each band, D) Angular integration of monochromatic transmittances over all angles is carried out by Gaussian quadrature and then the model coefficients are found, E) Band transmittance coefficients are found at nadir and then the transmittances are raised to the factor 1.66.

Table 4a

Comparison of OLR and DSF with ICRCCM Clear-sky Results

Case	OLR ($W \cdot m^{-2}$) Present Study	OLR ($W \cdot m^{-2}$) From ICRCCM	DSF ($W \cdot m^{-2}$) Present Study	DSF ($W \cdot m^{-2}$) From ICRCCM
Tropical	296.69	294.48[a]	394.46	389.89[a]
		298.28[b]		389.46[b]
		296.83[c]		389.96[c]
Midlatitude Summer	289.89	285.78[a]	344.84	342.31[a]
		288.99[b]		340.20[b]
		288.05[c]		343.23[c]
Midlatitude Winter	233.05	234.26[a]	217.78	215.42[a]
		236.56[b]		210.54[b]
		235.23[c]		217.27[c]
Subarctic Summer	266.52	266.29[a]	294.45	292.79[a]
		269.96[b]		287.31[b]
		269.44[c]		293.42[c]
Subarctic winter	200.16	200.87[a]	165.24	164.45[a]
		202.95[b]		162.45[b]
		201.27[c]		168.23[c]

a Line-by-line model - Schwarzkopf and Fels
b Line-by-line model - Scott and Chedin
c Line-by-line model - Arking A.

Table 4b

Comparison of OLR and DSF with ICRCCM Cloudy Results

Case	OLR ($W \cdot m^{-2}$) Present Study	OLR ($W \cdot m^{-2}$) From ICRCCM	DSF ($W \cdot m^{-2}$) Present Study	DSF ($W \cdot m^{-2}$) From ICRCCM
Cloud top at 13 km liquid water 10 $g \cdot m^{-2}$ effective dropsize 5.25 μm	163.76	165.06[a] 18.75 [b] 66.28[c]	359.05	360.43[a] 6.74[b] 23.10[c]
Cloud top at 2 km liquid water 10 $g \cdot m^{-2}$ effective dropsize 5.25 μm	275.19	276.05[a] 8.38[b] 33.68[c]	400.23	398.97[a] 8.02[b] 28.08[c]
Cloud top at 13 km liquid water 200 $g \cdot m^{-2}$ effective dropsize 31 μm	128.35	129.82[a] 5.26[b] 21.98[c]	361.16	361.10[a] 7.22[b] 24.22[c]
Cloud top at 2 km liquid water 200 $g \cdot m^{-2}$ effective dropsize 5.25 μm	271.02	273.47a 8.68[b] 39.67[c]	410.18	412.69[a] 2.54[b] 7.91[c]

a Mean value from the models included in the ICRCCM tests
b Standard Deviation from the mean
c Range of values found in the models

REPORT DOCUMENTATION PAGE

Form Approved
OMB No. 0704-0188

1. AGENCY USE ONLY *(Leave blank)*	2. REPORT DATE	3. REPORT TYPE AND DATES COVERED
	September 1999	Contractor Report

4. TITLE AND SUBTITLE
Longwave Radiation Flux Calculations in the TOVS Pathfinder Path A Data Set

5. FUNDING NUMBERS
910.4

6. AUTHOR(S)
A. Mehta and J. Susskind

7. PERFORMING ORGANIZATION NAME(S) AND ADDRESS (ES)
Laboratory for Atmospheres
Earth Sciences Directorate
Goddard Space Flight Center
Greenbelt, Maryland 20771

8. PEFORMING ORGANIZATION REPORT NUMBER
99B00065

9. SPONSORING / MONITORING AGENCY NAME(S) AND ADDRESS (ES)
National Aeronautics and Space Administration
Washington, DC 20546-0001

10. SPONSORING / MONITORING AGENCY REPORT NUMBER
CR—1999–208643

11. SUPPLEMENTARY NOTES
Mehta: General Sciences Corp.

12a. DISTRIBUTION / AVAILABILITY STATEMENT
Unclassified–Unlimited
Subject Category: 47
Report available from the NASA Center for AeroSpace Information,
7121 Standard Drive, Hanover, MD 21076-1320. (301) 621-0390.

12b. DISTRIBUTION CODE

13. ABSTRACT *(Maximum 200 words)*

A radiative transfer model developed to calculate outgoing longwave radiation (OLR) and downwelling longwave surface flux (DSF) from the Television and Infrared Operational Satellite (TIROS) Operational Vertical Sounder (TOVS) Pathfinder Path A retrieval products is described. The model covers the spectral range of 2 to 2800 cm^{-1} in 14 medium resolution spectral bands. For each band, transmittances are parameterized as a function of temperature, water vapor, and ozone profiles. The form of the band transmittance parameterization is a modified version of the approach we use to model channel transmittances for the High Resolution Infrared Sounder 2 (HIRS2) instrument. We separately derive effective zenith angle for each spectral band such that band-averaged radiance calculated at that angle best approximates directionally integrated radiance for that band. We develop the transmittance parameterization at these band-dependent effective zenith angles to incorporate directional integration of radiances required in the calculations of OLR and DSF. The model calculations of OLR and DSF are accurate and differ by less than 1% from our line-by-line calculations. Also, the model results are within 1% range of other line-by-line calculations provided by the Intercomparison of Radiation Codes in Climate Models (ICRCCM) project for clear-sky and cloudy conditions. The model is currently used to calculate global, multiyear (1985–1998) OLR and DSF from the TOVS Pathfinder Path A Retrievals.

14. SUBJECT TERMS
Longwave radiation; downwelling longwave surface flux; TIROS; TOVS.

15. NUMBER OF PAGES
21

16. PRICE CODE

17. SECURITY CLASSIFICATION OF REPORT	18. SECURITY CLASSIFICATION OF THIS PAGE	19. SECURITY CLASSIFICATION OF ABSTRACT	20. LIMITATION OF ABSTRACT
Unclassified	Unclassified	Unclassified	UL